Bioconjugate Chemistry

Article

pubs.acs.org/bc

^{64}Cu-Labeled LyP-1-Dendrimer for PET-CT Imaging of Atherosclerotic Plaque

Jai Woong Seo,[†] Hyounggee Baek,[†] Lisa M. Mahakian,[†] Jiro Kusunose,[†] Juliana Hamzah,[§] Erkki Ruoslahti,[‡] and Katherine W. Ferrara*[,†]

[†]Department of Biomedical Engineering, University of California, Davis, California 95616, United States

[‡]Cancer Research Center, Sanford-Burnham Medical Research Institute, La Jolla, California 92037, United States

[§]Western Australian Institute for Medical Research, Level 5, MRF Building, Rear, 50 Murray Street, Perth, WA 6000, Australia

Supporting Information

ABSTRACT: The ability to detect and quantify macrophage accumulation can provide important diagnostic and prognostic information for atherosclerotic plaque. We have previously shown that LyP-1, a cyclic 9-amino acid peptide, binds to p32 proteins on activated macrophages, facilitating the visualization of atherosclerotic plaque with PET. Yet, the in vivo plaque accumulation of monomeric [^{18}F]FBA-LyP-1 was low (0.31 ± 0.05%ID/g). To increase the avidity of LyP-1 constructs to p32, we synthesized a dendritic form of LyP-1 on solid phase using lysine as the core structural element. Imaging probes (FAM or 6-BAT) were conjugated to a lysine or cysteine on the dendrimer for optical and PET studies. The N-terminus of the dendrimer was further modified with an aminooxy group in order to conjugate LyP-1 and ARAL peptides bearing a ketone. Oxime ligation of peptides to both dendrimers resulted in $(LyP\text{-}1)_4$- and $(ARAL)_4$-dendrimers with optical (FAM) and PET probes (6-BAT). For PET-CT studies, $(LyP\text{-}1)_4$- and $(ARAL)_4$-dendrimer-6-BAT were labeled with ^{64}Cu ($t_{1/2}$ = 12.7 h) and intravenously injected into the atherosclerotic ($ApoE^{-/-}$) mice. After two hours of circulation, PET-CT coregistered images demonstrated greater uptake of the $(LyP\text{-}1)_4$-dendrimer-^{64}Cu than the $(ARAL)_4$-dendrimer-^{64}Cu in the aortic root and descending aorta. Ex vivo images and the biodistribution acquired at three hours after injection also demonstrated a significantly higher uptake of the $(LyP\text{-}1)_4$-dendrimer-^{64}Cu (1.1 ± 0.26%ID/g) than the $(ARAL)_4$-dendrimer-^{64}Cu (0.22 ± 0.05%ID/g) in the aorta. Similarly, subcutaneous injection of the LyP-1-dendrimeric carriers resulted in preferential accumulation in plaque-containing regions over 24 h. In the same model system, ex vivo fluorescence images within aortic plaque depict an increased accumulation and penetration of the $(LyP\text{-}1)_4$-dendrimer-FAM as compared to the $(ARAL)_4$-dendrimer-FAM. Taken together, the results suggest that the $(LyP\text{-}1)_4$-dendrimer can be applied for in vivo PET imaging of plaque and that LyP-1 could be further exploited for the delivery of therapeutics with multivalent carriers or nanoparticles.

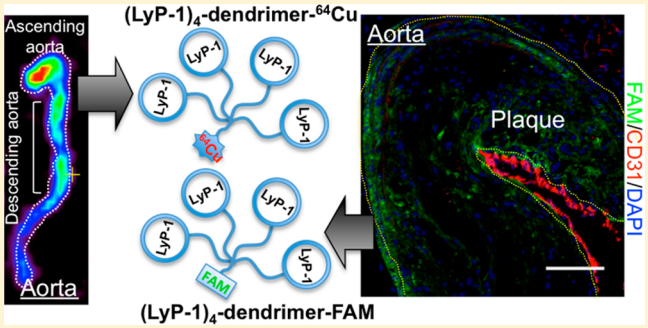

1. INTRODUCTION

Atherosclerosis, a chronic inflammatory vascular disease, is a high-risk factor for myocardial infarction and cerebrovascular events. Enlarged plaque lesions constrict the luminal surface of the artery and hence reduce blood flow.[1,2] Therefore, molecular imaging to monitor the progression of atherosclerosis can improve the management of patients and facilitate diagnosis.[3,4] Imaging modalities such as ultrasound,[5,6] computed tomography (CT),[7] magnetic resonance imaging (MRI),[8,9] single photon emission computed tomography (SPECT),[10,11] and positron emission tomography (PET)[12,13] have been exploited to visualize molecular changes in addition to anatomical structure.[14−16] To obtain a molecular readout of the lesion formation, PET is attractive due to the high sensitivity and the feasibility of dynamic studies. PET combined with MRI or CT is advantageous in cardiovascular imaging, as together they provide simultaneous images of molecular and anatomical information,[12,17] potentially improving diagnosis and patient management.

The formation of atherosclerotic plaque is associated with a complex biological progression which includes the production of multiple biomarkers.[1,2] Plaque macrophages and endothelial cells are considered to be the main targets for the noninvasive identification of atherosclerosis progression,[17−21] with vascular cell adhesion molecule-1 (VCAM-1) identified as a particularly important marker of early disease. [^{18}F]FDG, which accumulates in macrophages, has been applied to image inflammation associated with early atherosclerosis;[13,19,20] however, improvements in selective imaging of plaque are required to reduce the endogenous background.[21] Recently, ^{64}Cu-TNP (trireporter

Received: July 24, 2013
Revised: January 6, 2014
Published: January 16, 2014

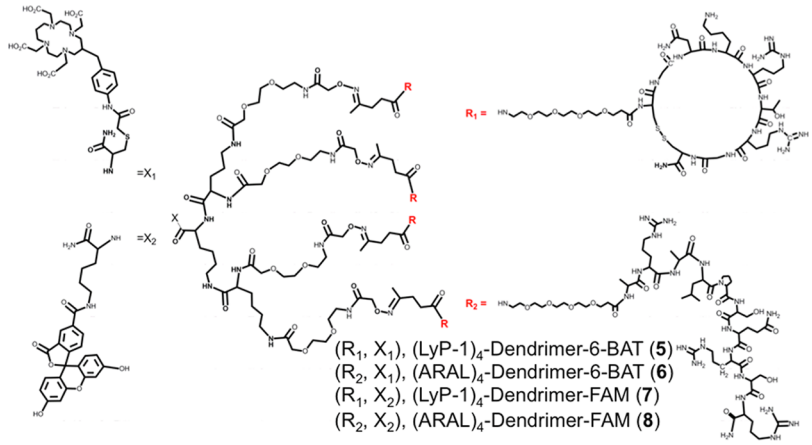

Figure 1. FAM- and 6-BAT-labeled LyP-1- and ARAL-dendrimers.

nanoparticles), which are dextran-coated nanoparticles including a near-infrared fluorochrome and ^{64}Cu, were specifically visualized on macrophages in inflammatory atherosclerosis and showed higher standard uptake values (SUV) than obtained with [^{18}F]FDG.[17]

LyP-1 (CGNKRTRGC), a cyclic peptide, recognizes tumor cells and macrophages by binding to the p32 protein on the cell surface.[22,23] Further, LyP-Hsp, a bioengineered protein cage expressing LyP-1, exhibited enhanced macrophage targeting.[24] Recently, Hamzah et al. demonstrated that LyP-1 is a promising peptide for targeting p32 that is overexpressed on plaque-associated macrophages.[25] In this study, F-18-labeled monomeric Lyp-1 selectively bound to atherosclerotic plaques and facilitated visualization of plaque with PET; however, the binding affinity (K_d = 3 μmol/L) of LyP-1 resulted in a relatively low accumulation (0.3%ID/g) in the aorta.[22,25] To address this issue, we designed and synthesized a dendrimer with multiple LyP-1 ligands on one scaffold, in a manner similar to other dendrimeric studies.[26] Multivalent dendrimers have been applied to increase the binding avidity of various targeting ligands.[27−29] Previously, tetrameric or pentameric dendrimers showed 4- to 300-fold greater avidity than monovalent peptides.[21,27,30,31] The enhanced avidity of such dendrimers has the potential to improve molecular imaging of atherosclerotic lesions.

Here, we designed and synthesized LyP-1 and control (ARALPSQRSR) dendrimers (Figure 1). Building blocks (peptides and core dendrimers including FAM (carboxyfluorescein or fluorescein amidite) or 6-BAT) were built on solid phase. Ammonium acetate catalyzed the hydrazone formation of peptides and dendrimers and produced the peptide-conjugated dendrimers, which facilitated fluorescent and PET-CT imaging of atherosclerotic plaque. Until now, quantitative studies of atherosclerotic plaque via p32 on macrophages have not been explored; therefore, here we evaluated the application of ^{64}Cu- and FAM-labeled dendrimers to image atherosclerotic plaque with PET-CT and fluorescence images.

2. MATERIALS AND METHODS

General Information and Materials. All Fmoc-amino acids, *O*-(7-azabenzotriazol-1-yl)-*N*,*N*,*N*′,*N*′-tetramethyluronium hexafluorophosphate (HATU), piperidine, *N*,*N*-diisopropylethylamine (DIPEA), 1,3-diisopropylcarbodiimide (DIC), 1-hydroxybenzotriazole (HOBt) and Rink amide MBHA resin (0.52 mmol/g) were purchased from Novabiochem (San Diego, CA) and AAPPTec (Louisville, KY). All other chemical reagents were obtained from commercial suppliers and used without further purification. Reversed-phase HPLC was performed on a Varian ProStar HPLC system with 220 and 254 nm UV detection, using a Microsorb C-12 semipreparative column (10 × 250 mm) at a flow rate of 4 mL/min, or a preparative column (25 × 250 mm) at a flow rate 13.5 mL/min. All runs used linear gradients of 5−30% buffer B in A (A: water containing 0.05% TFA, B: acetonitrile containing 0.05% TFA) over 40 min. Matrix assisted laser desorption ionization (MALDI) and electrospray ionization mass spectrometry (ESI-MS) were performed at the Campus Mass Spectrometry Facilities in the University of California, Davis. $CuCl_2$ was purchased from MIR Radiological Science at Washington University under a protocol controlled by the University of California, Davis. Schemes of the peptide building block synthesis are in the Supporting Information (SI-1).

Peptide Synthesis. The peptides [Lev-amido-dPEG$_4$-LyP-1 (LyP-1: C(S−S)GNKRTRGC-NH$_2$)] (**1**), [Lev-amido-dPEG$_4$-ARAL (ARAL: ARALPSQRSR-NH$_2$)] (**2**), FAM-dPEG$_4$-LyP-1 and FAM-dPEG$_4$-ARAL were prepared using standard Fmoc mediated solid-phase peptide synthesis on Rink amide MBHA resin (100 mg) using HATU (3 equiv) and DIPEA (6 equiv). All amino acids, *N*-Fmoc-amido-dPEG$_4$ acid and levulinic acid (Lev) were coupled with coupling reagents at room temperature for 45 min each. The carboxyfluorescein (10 equiv) was coupled with DIC (10 equiv, HOBt, 10 equiv) in DMF at room temperature overnight. For the disulfide bond, cyclization of LyP-1 was performed on resin with iodine (10 equiv) in DMF for 4 h before the coupling of the hydrophilic linker (*N*-Fmoc-amido-dPEG4 acid). The resin was washed with DMF (2 × 5 mL) and then three times with a copious volume of CH_2Cl_2, filtered, and dried in a vacuum. The resin was suspended in a mixture of TFA-H_2O-TIPS (95:2.5:2.5, v/v/v, total volume 5.0 mL) for 2.5 h. The peptide was purified on high performance liquid chromatography (HPLC) using 5−30% acetonitrile in water and 0.05% TFA, giving 35% yield from the crude peptide cleaved off from the resin. The correct purified product was confirmed by matrix-assisted laser desorption ionization (MALDI) under reflective mode or electron spray ionization (ESI): Lev-Amido-dPEG$_4$-LyP-1 (**1**): [M+H, $C_{52}H_{94}N_{19}O_{18}S_2$] calculated monoisotopic mass 1336.64, measured mass 1336.6, Lev-Amido-dPEG$_4$-ARAL (**2**): [M+H, $C_{62}H_{113}N_{22}O_{20}$] calculated monoisotopic mass 1485.85, measured mass 1485.8, FAM-dPEG$_4$-LyP-1 (LyP-1-

dx.doi.org/10.1021/bc400347s | *Bioconjugate Chem.* 2014, 25, 231−239

FAM): [M+H, $C_{68}H_{98}N_{19}O_{22}S_2$] calculated monoisotopic mass 1596.65, measured mass 1597.0.

Dendrimer Synthesis. *Synthesis of Dendrimer-6-BAT.* The resin (52 μmol, 1.0 equiv) was swollen in DMF in the peptide synthesizer reaction vessel for 1 h, followed by Fmoc deprotection and washed with DMF (3 × 3 mL), MeOH (2 × 3 mL) and DCM (2 × 3 mL). Fmoc-Cys(Trt)-OH (91.4 mg, 0.156 mmol, 3.0 equiv), HATU (59.3 mg, 0.156 mmol, 3.0 equiv) and DIPEA (54.3 μL, 0.312 mmol, 6.0 equiv) were added to the resin and the reaction mixture was agitated for 45 min at room temperature. The resin was washed with DMF (3 × 3 mL) and Fmoc removal was achieved by piperidine (20% v/v) in DMF (2 × 5 min) and washed with DMF (3 × 3 mL), MeOH (2 × 3 mL) and DCM(2 × 3 mL). Fmoc-Lys (Fmoc)-OH (92.3 mg, 0.156 mmol, 3.0 equiv), HATU (59.3 mg, 0.156 mmol, 3.0 equiv) and DIPEA (54.3 μL, 0.312 mmol, 6.0 equiv) were added to the resin and the reaction mixture was agitated for 45 min at room temperature. The resin was washed with DMF (2 × 3 mL) and the N-terminal Fmoc groups were deprotected with 20% piperidine-DMF solution (2 × 3 mL, 5 min each), followed by washing with DMF (3 × 3 mL), MeOH (2 × 3 mL) and DCM (2 × 3 mL). Fmoc-Lys(Fmoc)-OH (184 mg, 0.31 mmol, 6.0 equiv), HATU (118 mg, 0.31 mmol, 6.0 equiv) and DIPEA (109 μL, 0.62 mmol, 12.0 equiv) were added to the resin and the reaction mixture was agitated for 1 h. The resin was washed with DMF (3 × 3 mL), while the N-terminal Fmoc groups were deprotected with 20% (v/v) piperidine-DMF (2 × 3 mL, 7.5 min each) and washed with DMF (3 × 3 mL), MeOH (2 × 3 mL) and DCM (2 × 3 mL). Fmoc-mini-PEG-OH (241 mg, 0.62 mmol, 12.0 equiv), HATU (237 mg, 0.62 mmol, 12.0 equiv) and DIPEA (217 μL, 1.2 mmol, 24.0 equiv) were added to the resin and the reaction mixture was agitated for 90 min. The resin was washed with DMF (3 × 3 mL) and the N-terminal Fmoc groups were deprotected with 20% piperidine−DMF (v/v) and washed with DMF (3 × 3 mL), MeOH (2 × 3 mL) and DCM (2 × 3 mL). Boc-aminooxy acetic acid (123 mg, 0.64 mmol, 12.0 equiv), HATU (237 mg, 0.64 mmol, 12.0 equiv) and 2,4,6-trimethylpyridine (110 μL, 0.83 mmol, 16.0 equiv) were added to the resin and the reaction mixture was agitated for 90 min. The resin was washed with DMF (3 × 3 mL) and then three times with a copious volume of CH_2Cl_2, filtered, and dried in vacuum. The resin was suspended in a mixture of TFA-H_2O-TIPS (95: 2.5:2.5, v/v/v, total volume 3.0 mL) for 2.5 h and filtered to remove the resin. The cleavage cocktail was removed with a stream of N_2 and the crude product was precipitated with hexane:diethyl ether (1:1, v/v, 10 mL). The solvent was evaporated and the solid obtained was briefly dried in vacuum. The dendrimer was obtained after semipreparative HPLC and lyophilization. The product was confirmed by MALDI under reflective mode: dendrimer [M+H, $C_{53}H_{101}N_{16}O_{24}S$] calculated monoisotopic mass 1377.69, measured mass 1377.7.

6-BAT(6-[*p*-(bromoacetamido)benzyl]-1,4,8,11-tetraazacyclotetradecane-*N,N″,N‴,N⁗*-tetraacetic acid, 4.7 mg, 7.2 μmol) was attached to the dendrimer (10 mg, 7.2 μmol) via free thiol groups of C-terminal cysteine in 0.1 M ammonium acetate (pH 8.0) at room temperature for 6 h. The solution was lyophilized to obtain the solid. The dendrimer-6-BAT (**3**) conjugate (6.2 mg, 44%) was obtained after semipreparative HPLC using a gradient of acetonitrile in water (both containing 0.1% TFA) and lyophylization. The correct purified product was confirmed by MALDI under reflective mode: [M+H, $C_{80}H_{140}N_{21}O_{33}S$] where the calculated monoisotopic mass was 1954.96, measured mass 1955.3.

Synthesis of Dendrimer-FAM. The resin (52 μmol, 1.0 equiv) was swollen in DMF in the peptide synthesizer reaction vessel for 1 h, followed by Fmoc deprotection, and washed with DMF (3 × 3 mL), MeOH (2 × 3 mL) and DCM (2 × 3 mL). Fmoc-Lys(Mmt)-OH (100.0 mg, 0.156 mmol, 3.0 equiv), HATU (59.3 mg, 0.16 mmol, 3.0 equiv) and DIPEA (54.3 μL, 0.31 mmol, 6.0 equiv) were added to the resin and the reaction mixture was agitated for 45 min at room temperature. The resin was washed with DMF (3 × 3 mL) and Fmoc removal was achieved by piperidine (20% v/v) in DMF (2 × 3 min) and washed with DMF (3 × 3 mL), MeOH (2 × 3 mL) and DCM (2 × 3 mL). The following reactions were performed as described above until the deprotection of Mmt was achieved. The N-terminal Mmt groups were deprotected in a mixture of AcOH-TFE-DCM (1:2:7, v/v/v, 5 mL) and washed with DMF (3 × 3 mL), MeOH (2 × 3 mL) and DCM (2 × 3 mL). The 5(6)-carboxyfluorescein (58.7 mg, 0.156 mmol, 3.0 equiv), HATU (59.3 mg, 0.16 mmol, 3.0 equiv) and DIPEA (54.3 μL, 0.31 mmol, 6.0 equiv) dissolved in DMF were added to the resin and the reaction mixture was agitated for 10 h. The resin was washed with DMF (3 × 3 mL) and then three times with a copious volume of CH_2Cl_2, filtered, and dried in vacuum. The resulting material was suspended in a mixture of TFA-H_2O-TIPS (95: 2.5:2.5, v/v/v, total volume 3.0 mL) for 2.5 h and filtered to remove the resin. The cleavage cocktail was removed with a stream of N_2 and the crude product was precipitated with hexane:diethyl ether (1:1, v/v, 10 mL). The solvent was evaporated and the solid obtained was briefly dried in vacuum. Dendrimers were obtained after semipreparative HPLC using a gradient of acetonitrile in water (both containing 0.1% TFA) and lyophilization. The product was confirmed by MALDI under reflective mode: dendrimer-FAM (**4**): [M+H, $C_{77}H_{118}N_{17}O_{30}$] calculated monoisotopic mass 1760.82, measured mass 1760.6.

Synthesis of Peptide-Dendrimers via Oxime Ligation. Six equivalents of the levulinic acid-functionalized peptides were incubated overnight with 1 equiv of dendrimer-6-BAT or dendrimer-FAM (2−7 μmol scale) in 100 mM anilinium acetate (pH 4.5). The products were purified by semipreparative HPLC using a gradient of acetonitrile in water (both containing 0.1% TFA) and lyophilization. The isolated yield was 57 ± 9%. The product confirmed by MALDI under linear mode: $(LyP\text{-}1)_4$-dendrimer-6-BAT (**5**): [M+H, $C_{288}H_{504}N_{97}O_{101}S_9$] calculated mass 7230.28, measured mass 7237.7, $(ARAL)_4$-dendrimer-6-BAT (**6**): [M+H, $C_{328}H_{580}N_{109}O_{109}S$] calculated mass 7826.87, measured mass 7837.5. $(LyP\text{-}1)_4$-dendrimer-FAM (**7**): [M+H, $C_{285}H_{482}N_{93}O_{98}S_8$] calculated mass 7035.98, measured mass 7045.5, $(ARAL)_4$-dendrimer-FAM (**8**): [M+H, $C_{325}H_{558}N_{105}O_{106}$] calculated mass 7632.56, measured mass 7642.5.

Preparation of ^{64}Cu-Labeled LyP-1- and ARAL-Dendrimers. All labeling procedures were controlled under a protocol of the University of California, Davis. To a solution of $^{64}CuCl_2$ buffered with 0.1 M ammonium citrate (pH 5.5, 0.2 mL), we added 1 mM $(LyP\text{-}1)_4$- and $(ARAL)_4$-dendrimer-6-BAT (2−4 μmol) in double distilled water with a 37 MBq/nmol concentration. The mixture was incubated at 30 °C for 1 h and the reaction completion was monitored by radio-TLC. The reaction mixture was diluted with double distilled water (6 mL) and the pH was adjusted to 7 with 1 M sodium hydroxide solution. The solution was drawn into the syringe and was

dx.doi.org/10.1021/bc400347s | *Bioconjugate Chem.* 2014, 25, 231−239

passed dropwise through the preactivated light Sep-Pack C18 plus light cartridge (Waters, Milford, MA). The cartridge was washed with double distilled water (10 mL × 2) dropwise. The product trapped on a C18 cartridge was recovered by a releasing solution (<0.7 mL of 1% AcOH, 80% EtOH, 19% H_2O, volume %). The solvent was evaporated under nitrogen at 60 °C until dry (<30 min). After assessing the dryness of the compound, the isolated dendrimer was resuspended in PBS. The radiochemical purity was determined by radio-TLC and HPLC (SI-3).

Saturation Binding Assay. LyP-1-dendrimer binding affinity (K_d) to p32 protein was quantified by a sandwich ELISA-based assay. 96 well plates (Costar EIA/RIA 1 × 8 Stripwell plate, Corning Inc., NY) with 5 μg/mL of p32 protein (R&D systems, MN) were incubated with varied concentrations (1 μM − 1 nM) of $(LyP\text{-}1)_4$-dendrimer-^{64}Cu (100 μL in PBS) for 1 h at room temperature. After washing with 0.05 wt % Tween 10 in PBS, the radioactivity of each well was counted on a gamma counter (Perkin-ElmerLife Sciences). Nonspecific binding of the LyP-1-dendrimer was measured by spiking 0.1 mM nonlabeled $(LyP\text{-}1)_4$-dendrimer-6-BAT in various concentrations of $(LyP\text{-}1)_4$-dendrimer-^{64}Cu. Experiments were duplicated and the K_d value was calculated by Prism (SI-5).

In Vivo Imaging and Biodistribution Studies. All animal experiments were conducted under a protocol approved by the University of California, Davis, Animal Use and Care Committee (Davis, CA). ApoE-null mice (The Jackson Laboratory, Bar Harbor, ME) with atherosclerotic plaques were induced by maintenance on a high fat diet for 6 months and were supplied to us by the University of California, Santa Barbara. A total of n = 22 mice were studied, where 16 mice were injected with the $(Lyp\text{-}1)_4$-dendrimer-^{64}Cu (n = 9) and $(ARAL)_4$-dendrimer-^{64}Cu (n = 7) for both PET imaging and biodistribution and 6 mice were injected with $(Lyp\text{-}1)_4$-dendrimer-FAM (n = 2), Lyp-1-FAM (n = 2) and $(ARAL)_4$-dendrimer-FAM (n = 2) for optical imaging. All imaging was conducted under 1.5% isoflurane.

PET-CT Imaging and Biodistribution. For the PET-CT study, ^{64}Cu-dendrimers were administered to ApoE$^{-/-}$ mice through the tail vein and images were acquired at 2 h after injection. For studies involving biodistribution after intravenous (IV) injection, ApoE$^{-/-}$ mice received 6.6 ± 1.3 MBq of the $(Lyp\text{-}1)_4$-dendrimer-^{64}Cu (n = 6) or 7.1 ± 1.7 MBq of the $(ARAL)_4$-dendrimer-^{64}Cu (n = 4). The average mass of the LyP-1 and ARAL-dendrimer injected was 2.7 ± 1.3 μg (n = 9) and 2.6 ± 1.3 μg (n = 8), respectively. For studies in which the mice received the dose subcutaneously, 15.1 ± 3.1 MBq (n = 3) of the $(Lyp\text{-}1)_4$-dendrimer-^{64}Cu and 10.6 ± 6.2 MBq (n = 3) of $(ARAL)_4$-dendrimer-^{64}Cu were administered and the mice were euthanized at 24 h after injection. At each time point, two mice were imaged simultaneously for 20 min on the PET scanner (Focus 120, Siemens Medical Solutions, Inc.). After data acquisition with PET, mice were carefully moved to a commercially available micro CT scanner, MicroCAT II (Siemens, Knoxville, TN) operated in high resolution mode with a 0.5 mm aluminum filter. One hundred eighty projections were acquired during a full rotation with the following scan parameters: 80 kVp, 425 μA, 240 ms per frame and 30 calibration images. The total scan time for one bed position was 15 min. PET images were reconstructed using the MAP algorithm with 1.5 mm spatial resolution. CT images were reconstructed using the Feldkamp reconstruction algorithm as a 896 × 512 × 1024 array with corresponding pixel size of 0.098 mm × 0.098 mm × 0.098 mm (x,y,z) with 43 μm spatial resolution. PET and CT images were fused with AMIDE (AMIDE's Medical Image Data Examiner) using three fiducials placed on the bed. The aortic root and aortic arch (Figure 2)

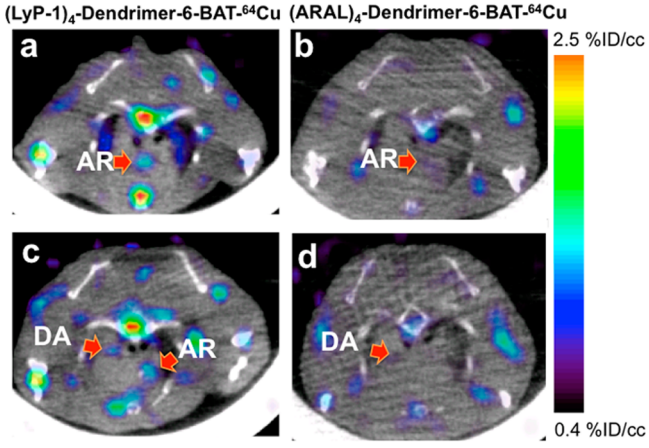

Figure 2. Co-registered PET-CT images acquired after 2 h administration of $(LyP\text{-}1)_4$-dendrimer-^{64}Cu (a and c, left column) and $(ARAL)_4$-dendrimer-^{64}Cu (b and d, right column). Red arrow indicates aortic root (AR) and descending aorta (DA).

were identified by their relative position within the 3D data set and relative image intensity. For the ex vivo PET study, the excised aorta was placed on a polyacryl (50 mmID) transparent dish and was covered with OCT to prevent dryness. Ex vivo PET images of the aorta were acquired for 30 min. Image reconstruction followed the protocol mentioned above.

To evaluate the pharmacokinetics following subcutaneous injection of the dendrimers, ^{64}Cu-dendrimers were subcutaneously injected in the loose skin of the neck of ApoE$^{-/-}$ mice (n = 3 for $(Lyp\text{-}1)_4$-dendrimer, n = 3 for $(ARAL)_4$-dendrimer). Image acquisition was performed at 24 h for 20 min on Focus120 (Siemens Medical Solutions, Inc.) and ex vivo PET imaging of the aorta followed the same procedure as above.

The biodistribution was then acquired after the imaging studies described above. In each case, mice were euthanized with euthasol (Western Medical Supply, Arcadia,CA) at 3 h. The blood was perfused from the body with DMEM (Invitrogen, Carlsbad, CA). Organs, including the lymph nodes, aorta, heart, were then harvested and the biodistribution and radioactivity were measured in a gamma counter (Perkin-ElmerLife Sciences).

Ex Vivo Optical Imaging of the Aorta with FAM Labeled Dendrimers and LyP-1-FAM. $(LyP\text{-}1)_4$-dendrimer-FAM, $(ARAL)_4$-dendrimer-FAM and LyP-1-FAM were prepared as 1 μmol/mL in PBS. Each 150 μL of solution was injected to ApoE$^{-/-}$ mice through the tail vein. After circulation for 1 h, blood was perfused with saline and tissues were fresh frozen in OCT. Microscopic optical images of the plaque in the aorta were acquired at randomly selected locations. The detailed procedure followed previously reported literature.[25] For image analysis of accumulated dendrimers in plaque, the TIFF images of the cross sectional area of the aorta were processed in Image J (v 1.46r, NIH USA). Regions of interest (ROI) were drawn over the composite image (RGB) between endothelial and smooth muscle cells within the plaque. The

dx.doi.org/10.1021/bc400347s | Bioconjugate Chem. 2014, 25, 231−239

green channel was extracted from the image and the mean pixel intensity was calculated.

3. RESULTS AND DISCUSSION

Synthesis of LyP-1- and ARAL-Dendrimer. L-Lysine, a natural amino acid which has two primary reactive amines, has been exploited as a branch unit for dendrimers[32,33] because of advantages including (1) the commercial availability of orthogonally protected amines on the lysine which allow a selective modification of α- and ε-amines, (2) the feasibility of solid phase synthesis, and (3) the relatively low cytotoxicity as a dendrimeric scaffold.[34] We therefore followed the building block approach illustrated in Figures 1 and 2 in which the peptide and dendrimer were synthesized separately on resin and finally conjugated in solution phase for the efficient synthesis of the peptide-conjugated dendrimer.

Altogether, we designed four building blocks (Scheme 1 and Figure 1); two are dendrimers conjugated with 6-BAT and FAM for PET and optical studies, respectively, and two include LyP-1 (**1**) and ARAL peptides (**2**, LyP-1 and the control peptide each have a +3 charge). Among possible methods for orthogonal conjugation of the peptides and dendrimer, including click reactions,[28] thioether methods,[29,35] and hydrazone formation, we followed oxime ligation because oxime ligation has demonstrated successful conjugation of ketone and aminooxy groups in an anilinium acetate buffer.[26] First, monomethoxytrityl (Mmt) protected cysteine (Fmoc-Cys(Mmt)-OH) or lysine (Fmoc-Lys(Mmt)-OH) was coupled on the resin; Mmt was later deprotected before reacting with 6-BAT or carboxyfluorescein (FAM). The dendritic scaffold was formed by two cycles of a coupling reaction of Fmoc protected lysine. The four amine residues were then extended with miniPEG (poly(ethylene glycol)) and Boc protected aminooxyacetic acid. Cleavage of dendrimers followed by HPLC purification gave aminooxy functionalized dendrimer-6-BAT and -FAM (Figure 1).

Scheme 1. Syntheses of LyP-1- and ARAL-Dendrimers from Building Blocks[a]

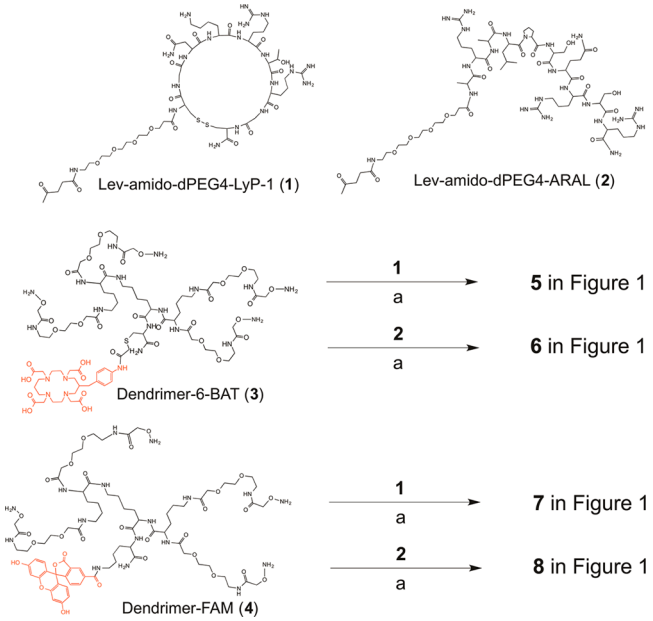

[a]Reagents, conditions and yield: (a) anilinium acetate (0.1 M, pH 4.5), room temperature, overnight, **5** (45%), **6** (59%), **7** (63%), and **8** (63%).

For the solid phase synthesis of Lev-amido-dPEG$_4$-LyP-1 (**1**), Fmoc-NH-CGNKRTRGC was cyclized on a resin with iodine before coupling with dPEG$_4$ and levulinic acid. The linear Lev-amido-dPEG$_4$-ARAL was synthesized on a resin by routine Fmoc chemistry. A PEG-spacer was placed between the levulinic acid and peptides to reduce the steric hindrance of the cyclic peptide and to increase the accessibility of ketone group in Lev to the aminooxy group on the dendrimer. Overnight incubation of dendrimer-6-BAT (**3**) with 6 equiv of Lev-amido-dPEG$_4$-LyP-1 (**1**) and Lev-amido-dPEG$_4$-ARAL (**2**) in anilinium acetate (0.1 M, pH 4.5) yielded the expected (LyP-1)$_4$-dendrimer-6-BAT (**5**) and (ARAL)$_4$-dendrimer-6-BAT (**6**), respectively, which was confirmed by MALDI mass spectroscopy (Figure SI-2). For (LyP-1)$_4$-dendrimer-FAM (**7**) and (ARAL)$_4$-dendrimer-FAM (**8**), although HPLC purification showed one peak via the UV detector, the MALDI spectrum from that fraction showed multiple mass peaks of mono-, di, tri, and tetra-peptide conjugated dendrimers (Figure SI-2.8 and 2.9).

Preparation of (LyP-1)$_4$- and (ARAL)$_4$-Dendrimer-^{64}Cu. Several ^{64}Cu chelators have been developed to label larger molecules such as peptides, dendrimers, antibodies, albumin, and nanoparticles.[36] Here, we used 6-BAT for PET imaging studies of the targeted dendrimer. Our group previously demonstrated the feasibility of chelating 6-BAT with ^{64}Cu in nanoparticles.[37,38] The resulting radiolabeled nanoparticle was stable in blood for more than 24 h, and therefore this chelation approach was considered to be adequate for imaging the pharmacokinetics of the lower molecular weight dendrimer (7−8 kDa) which is expected to have a short blood half-life. The selectivity of 6-BAT for copper (as compared with other metal contaminants) facilitates a high specific activity dendrimer.[39]

Radiolabeling of both dendrimers with $^{64}CuCl_2$ was performed in ∼37 MBq/nmol (^{64}Cu/dendrimer) due to the specific activity of ^{64}Cu (55.5−740 MBq/nmol).[40,41] Incubation for one hour at 30 °C showed more than 94% incorporation yield (n = 6) on radio-thin layer chromatography (radio-TLC). The calculated specific activity of the (LyP-1)$_4$- and (ARAL)$_4$-dendrimer-^{64}Cu at the end of the synthesis was 26.5 ± 4.7 (n = 3) and 26.3 ± 5.8 MBq/nmol (n = 3), respectively. Decay corrected radiochemical yield (n = 3) of the (LyP-1)$_4$- and (ARAL)$_4$-dendrimer-^{64}Cu was 80 ± 5.7% and 78 ± 6.4%, respectively. The radiochemical purity of the dendrimers was >95% confirmed by radio-TLC and radio-HPLC (Figure SI-3).

Saturation Binding Assay of (LyP-1)$_4$-Dendrimer-^{64}Cu. Previously, LyP-1 peptide showed a binding affinity of 3 μM with p32 proteins.[22] Here, the saturation binding assay of (LyP-1)$_4$-dendrimer-^{64}Cu with p32 protein showed a binding affinity of K_d = 169 nM, which is 20-fold higher than the LyP-1 peptide.

In Vivo PET-CT Imaging of Atherosclerotic Plaque with (LyP-1)$_4$-Dendrimer-^{64}Cu and Biodistribution. Recently, Nahrendorf et al. used PET-CT to show that dextran-coated superparamagnetic, fluorescent, and ^{64}Cu-labeled nanoparticles localized to macrophages in atherosclerotic plaques.[17] However, the targeting mechanism was postulated to be the high inherent phagocytic avidity. With the small dendrimeric structures used here, phagocytic activity is expected to be reduced as compared with larger nanotherapeutics.

dx.doi.org/10.1021/bc400347s | Bioconjugate Chem. 2014, 25, 231−239

Our previous plaque imaging approach involved targeting p32 proteins on macrophages with the [^{18}F]-FBA-LyP-1 peptide in ApoE$^{-/-}$ mice and visualizing the anatomical location via PET.[25] In the current work, coregistered PET-CT images of ApoE$^{-/-}$ mice which received the (LyP-1)$_4$-dendrimer-^{64}Cu showed a robust PET signal in the aortic root and descending aorta (Figure 2a,c). Accumulation of the (ARAL)$_4$-dendrimer-^{64}Cu in ApoE$^{-/-}$mice was not significantly greater than background (Figure 2b,d). Aortic radioactivity associated with the LyP-1-dendrimer was 1.1 ± 0.26%ID/g, which was significantly higher than activity resulting from injection of the (ARAL)$_4$-dendrimer-^{64}Cu (0.22 ± 0.05%ID/g) (Figure 3b and Table 1). Furthermore, the aorta/blood ratio of

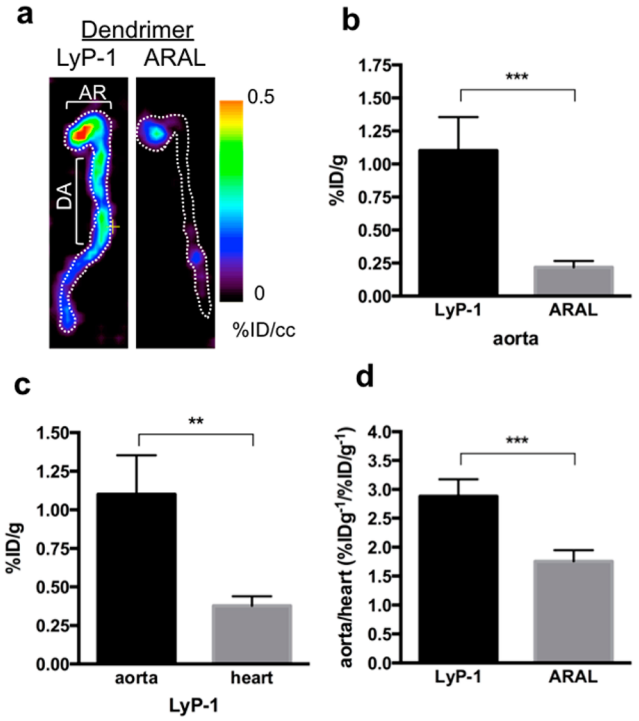

Figure 3. Ex vivo imaging and biodistribution study at 3 h after IV injection of (LyP-1)$_4$-dendrimer-^{64}Cu and (ARAL)$_4$-dendrimer-^{64}Cu. (a) Ex vivo PET images of excised aorta treated with (LyP-1)$_4$-dendrimer-^{64}Cu and (ARAL)$_4$-dendrimer-^{64}Cu. (b) Percent injected dose per gram (%ID/g) in the aorta in ApoE$^{-/-}$ mice. The accumulation of the (LyP-1)$_4$-dendrimer was significantly greater than the (ARAL)$_4$-dendrimer (P < 0.001). (c) Comparison of (LyP-1)$_4$-dendrimer associated radioactivity in the aorta and heart indicates that the %ID/g in the aorta was significantly higher than that in heart. (d) The signal (aorta) to background (heart) ratio of LyP-1-dendrimer and ARAL dendrimer.

the (LyP-1)$_4$-dendrimer-^{64}Cu (3.67 ± 1.07%ID/g, n = 6) was significantly higher than that of [^{18}F]FBA-LyP-1 (1.21 ± 0.37% ID/g, n = 4) (p = 0.002) (Figure SI-4.1). The significantly lower background signal from blood facilitates detection of plaque within in vivo PET images.

Following venous administration, the excised aorta from the PET images of the (LyP-1)$_4$-dendrimer-^{64}Cu-treated ApoE$^{-/-}$ mice (Figure 3a) showed higher activity in the aortic arch and descending aorta than mice treated with (ARAL)$_4$-dendrimer-^{64}Cu. Further, the accumulation of the (LyP-1)$_4$-dendrimer-^{64}Cu in the aorta was significantly higher than in the heart (Figure 3c, p < 0.01). Also, based on the biodistribution, the accumulation of the (LyP-1)$_4$-dendrimer-^{64}Cu in the aorta was 3-fold higher than the closely adjacent heart (Figure 3d) and 8-fold higher than in skeletal muscle (Table 1). The accumulation of (LyP-1)$_4$-dendrimer-^{64}Cu, as compared with the (ARAL)$_4$-dendrimer-^{64}Cu, demonstrates that the LyP-1-dendrimer specifically binds to plaque (Figure 3d).

Table 1. Biodistribution of (LyP-1)$_4$- and (ARAL)$_4$-Dendrimer-^{64}Cu at 3 h after Intravenous Injection in ApoE$^{-/-}$ Mice[a]

	(LyP-1)$_4$-dendrimer-^{64}Cu (ApoE$^{-/-}$, n = 6)		(ARAL)$_4$-dendrimer-^{64}Cu (ApoE$^{-/-}$, n = 4)	
organs	mean	std	mean	std
blood**	0.31	0.071	0.13	0.023
lungs**	1.22	0.38	0.37	0.038
liver	15.75	4.0	15.23	3.5
spleen	3.25	0.62	2.90	0.76
kidneys	88.41	27.8	54.46	17.4
renal LNs	1.40	0.59	2.08	0.33
inguinal LN	1.22	0.31	0.88	0.26
axillary LN	1.12	0.29	1.05	0.26
lumbar LN	1.56	0.72	2.14	1.25
pancreas***	0.65	0.073	0.22	0.052
cecum	0.52	0.25	0.26	0.079
intestine**	1.10	0.30	0.52	0.14
stomach*	0.48	0.22	0.16	0.035
muscle***	0.15	0.040	0.04	0.011
heart***	0.38	0.060	0.12	0.022
aorta***	1.10	0.26	0.22	0.049
aorta/muscle[b]	7.95	2.73	5.81	1.30

[a]Accumulation in %ID/g unless otherwise noted. *P < 0.05; ** P < 0.01; *** p < 0.001; LN, Lymph node. [b](%ID/g)/(%ID/g).

It has been reported that a positive charge on particles enhanced uptake by osteoblastic[42,43] and mesenchymal stem cells.[44] Although our results do not involve similar particles, the net charge on (LyP-1)$_4$- and (ARAL)$_4$-dendrimers, each +12, could potentially increase bone uptake, and some bone accumulation was observed on PET-CT images (Figure 2). We hypothesize that the greater bone uptake of the (LyP-1)$_4$-dendrimer-^{64}Cu, as compared to the (ARAL)$_4$-dendrimer-^{64}Cu, may result from receptor-mediated binding. The uptake of the (LyP-1)$_4$-dendrimer-FAM observed in the spine demonstrated that the accumulation of the (LyP-1)$_4$-dendrimer-FAM in bone was greater than that of (ARAL)$_4$-dendrimer-FAM and LyP-1-FAM (SI-4: Figure SI-4.2).

The biodistribution of the (LyP-1)$_4$- and (ARAL)$_4$-dendrimer-^{64}Cu was then assessed in ApoE$^{-/-}$ mice (n = 10) (Tables 1 and 2). Three hours after the administration of dendrimers, the residual radioactivity of (LyP-1)$_4$-dendrimer-^{64}Cu in the clearance organs (liver, spleen and kidneys) was not significantly different from that of the (ARAL)$_4$-dendrimer-^{64}Cu (Table 1). This is also in agreement with previous reports that the distribution of peptides [^{18}F]FBA-LyP-1 and [^{18}F]FBA-ARAL in these organs was not significantly different [25] and that the FAM-labeled LyP-1-targeted dendritic wedge was not specifically homing to the kidney.[26] The higher uptake of the (LyP-1)$_4$-dendrimer-^{64}Cu in clearance organs (liver, spleen and kidneys; Table 1) as compared with [^{18}F]FBA-LyP-1[25] might result from differences in the molecular size. The uptake of both dendrimers was similar in the lymph nodes. The results indicate that the accumulation in other lymphatic tissues was not receptor

dx.doi.org/10.1021/bc400347s | Bioconjugate Chem. 2014, 25, 231−239

Table 2. Biodistribution of $(LyP\text{-}1)_4$- and $(ARAL)_4$-Dendrimer-^{64}Cu at 24 h after Subcutaneous Injection in $ApoE^{-/-}$ Mice[a]

	$(LyP\text{-}1)_4$-dendrimer-^{64}Cu ($ApoE^{-/-}$, n = 3)		$(ARAL)_4$-dendrimer-^{64}Cu ($ApoE^{-/-}$, n = 3)	
organs	mean	std	mean	std
blood*	0.40	0.19	0.26	0.080
renal LNs	1.04	0.29	1.08	0.44
cecum*	1.43	0.25	0.92	0.12
pancreas	0.46	0.26	0.19	0.052
liver	6.32	1.7	8.66	3.4
spleen	1.32	0.43	1.23	0.61
kidneys*	21.5	2.4	14.96	2.8
inguinal LN	0.52	0.06	0.62	0.023
axillary LN	0.67	0.18	0.77	0.50
lumbar LN	0.62	0.21	0.74	0.37
lungs**	1.02	0.028	0.58	0.090
Intestine	1.17	0.39	0.61	0.047
stomach*	0.77	0.11	0.40	0.13
muscle	0.09	0.032	0.08	0.054
heart	0.59	0.11	0.34	0.12
aorta*	0.53	0.12	0.25	0.092
aorta/muscle[b]	6.14	1.5	3.42	0.84

[a]Accumulation in %ID/g unless otherwise noted. *P < 0.05; ** P < 0.01; *** p < 0.001; LN: Lymph node. [b](%ID/g)/(%ID/g).

mediated but instead represented passive uptake. Further, greater radioactivity resulting from injection of the $(LyP\text{-}1)_4$-dendrimer-^{64}Cu was also detected in digestive organs such as the pancreas (3-fold, p > 0.001), intestines (2-fold, p > 0.001), and stomach (3-fold, p > 0.05), compared to that from injection of $(ARAL)_4$-dendrimer-^{64}Cu.

When dendrimers are conjugated with biological therapeutics, extended circulation and local accumulation are desired. Therefore, subcutaneous administration may be preferable to intravenous injection and is currently utilized in clinical studies of miRNA efficacy. Further, enhanced accumulation within the plaque has the potential to reduce the required injected dose and therefore greatly reduce the cost of treatment. To evaluate the transport of the dendrimer in the subcutaneous space and the release into the blood pool, we performed a biodistribution study over 24 h after subcutaneous injection of the $(LyP\text{-}1)_4$- and $(ARAL)_4$-dendrimer-^{64}Cu. Twenty four hours following subcutaneous injection, aortic radioactivity (LyP-1: 0.53 ± 0.12%ID/g and ARAL: 0.25 ± 0.09%ID/g) resulting from injection of the $(LyP\text{-}1)_4$-dendrimer-^{64}Cu was higher than that of $(ARAL)_4$-dendrimer-^{64}Cu (Figure 5b, p = 0.033). Ex vivo imaging of aortas with PET (Figure 4a) confirmed the higher accumulation of radioactivity in the aortic arch from $(LyP\text{-}1)_4$-dendrimer-^{64}Cu injected $ApoE^{-/-}$ mice as compared with the ARAL-conjugated dendrimer. In addition, the accumulation of radioactivity associated with the $(LyP\text{-}1)_4$-dendrimer-^{64}Cu was approximately 6-fold greater in the aorta than in muscle.

At the same time point, radioactivity in the heart (0.59 ± 0.11%ID/g) and aorta (0.53 ± 0.12%ID/g) was similar (Figure 4c,d). The results support the hypothesis that the subcutaneous injection of targeted dendrimers could produce a sustained delivery of conjugated therapeutics to atherosclerotic plaque. Otherwise, with the exception of the stomach, lung, kidneys, and blood, radioactivity resulting from the LyP-1- and ARAL-dendrimers was similar (Table 2).

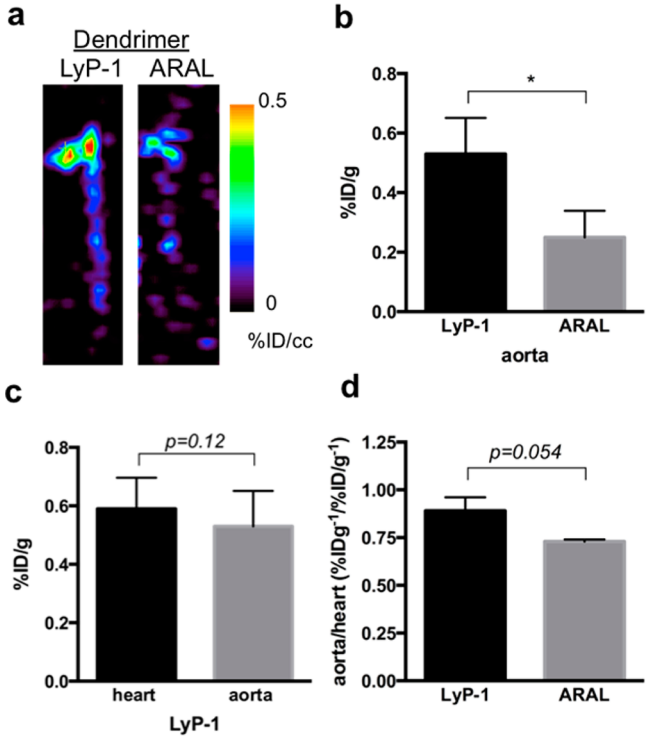

Figure 4. Ex vivo imaging and biodistribution study at 24 h after subcutaneous injection of $(LyP\text{-}1)_4$-dendrimer-^{64}Cu and $(ARAL)_4$-dendrimer-^{64}Cu. (a) Ex vivo PET images of excised aorta treated with $(LyP\text{-}1)_4$-dendrimer-^{64}Cu and $(ARAL)_4$-dendrimer-^{64}Cu. (b) Percent injected dose per gram (%ID/g) in the aorta of $ApoE^{-/-}$ mice. Accumulation of the $(LyP\text{-}1)_4$-dendrimer-^{64}Cu in the aorta was higher than the $(ARAL)_4$-dendrimer-^{64}Cu (P < 0.001). (c) LyP-1 associated radioactivity in the aorta and heart was not significantly different. (d) Signal (aorta) to background (heart) ratio of the $(LyP\text{-}1)_4$-dendrimer-^{64}Cu and $(ARAL)_4$-dendrimer-^{64}Cu.

Fluorescence Imaging Study of Atherosclerotic Plaque with FAM Labeled LyP-1, $(LyP\text{-}1)_4$-Dendrimer-FAM and $(ARAL)_4$-Dendrimer-FAM. Our previous study showed that LyP-1-FAM penetrated into the plaque interior. Here, we also evaluated the distribution of two dendrimers and the LyP-1 peptide labeled with 5(6)-carboxy fluorescein (FAM). Plaque retention and distribution were greater for the $(LyP\text{-}1)_4$-dendrimer-FAM as compared to the $(ARAL)_4$-dendrimer-FAM (Figure 5a,b). Analysis of optical images of plaque (Figure 5d) demonstrated a significantly higher mean pixel intensity (MPI) of $(LyP\text{-}1)_4$-dendrimer-FAM (30.3 ± 5.8 MPI, p = 0.01) and LyP-1-FAM (18.7 ± 4.04 MPI, p = 0.012) than $(ARAL)_4$-dendrimer-FAM (3.46 ± 1.6 MPI).

Based on the biodistribution data for the entire aorta, the uptake of the $(LyP\text{-}1)_4$-dendrimer-^{64}Cu (1.1%ID/g) was 3.5-fold higher than [^{18}F]FBA-LyP-1 (0.31%ID/g).[25] Based on region of interest analysis from optical imaging, the local accumulation of a $(LyP\text{-}1)_4$-dendrimer-FAM (30.3 ± 5.8 MPI) in plaque, calculated as the MPI value, was higher than monomeric LyP-1-FAM (18.7 ± 4.04 MPI) (Figure 5 and Figure SI-4.3); however, the difference was not significant (p = 0.054, Figure 5d). Given that the PET biodistribution demonstrated a significant difference, the lack of significance with optical imaging likely results from challenges in quantifying the fluorescent intensity. In part, this may result from image saturation at the vessel wall and autofluorescence of vascular tissues. The result was agreement with previous studies

dx.doi.org/10.1021/bc400347s | Bioconjugate Chem. 2014, 25, 231−239

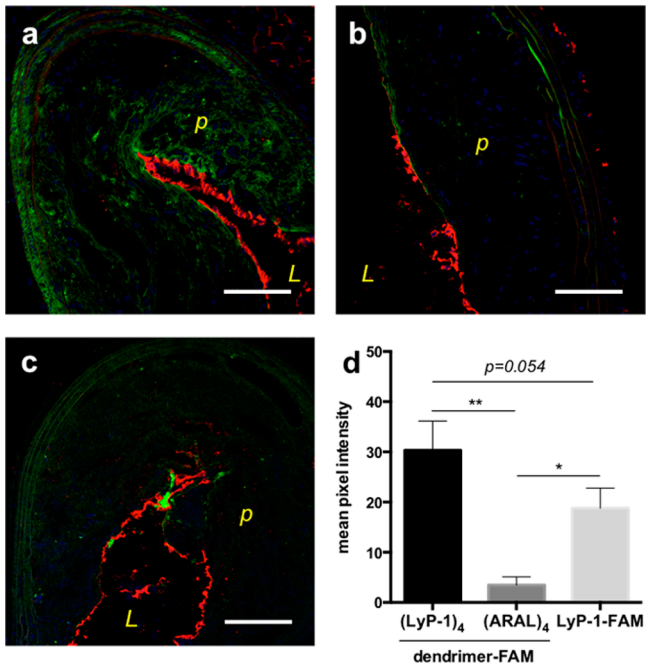

Figure 5. Representative microscopic images of aorta containing plaques (i.e., 7 μm tissue cross sections) 1 h after intravenous injection of (a) $(LyP\text{-}1)_4$-dendrimer-FAM, (b) $(ARAL)_4$-dendrimer-FAM, and (c) LyP-1-FAM, in atherosclerotic mice. Green channel: FAM labeled dendrimer or peptide; red channel: luminal endothelium (anti-CD31); blue channel: nuclei (DAPI) (Scale bars, 100 μm). The *P* and *L* represent plaque and lumen, respectively. (d) Mean pixel intensity of green fluorescence from the ROI (region of interest) of plaque. ($(LyP\text{-}1)_4$-dendrimer-FAM (n = 3), $(ARAL)_4$-dendrimer-FAM (n = 2), LyP-1-FAM (n = 3), ** = $P < 0.001$, * = $P < 0.05$).

in which a LyP-1-wedge with a mass of 10 kDa was efficiently internalized into tumor cells.[26] Taken together, the results suggest that multimeric LyP-1 could increase drug delivery to plaque, enhancing the drug local concentration.

4. CONCLUSION

We visualized atherosclerotic plaque in $ApoE^{-/-}$ mice with PET-CT and optical imaging using p32-targeted dendrimers. The $(LyP\text{-}1)_4$-dendrimer-BAT was successfully synthesized and labeled with ^{64}Cu and enhanced accumulation as compared with the monomeric peptide. Although FAM-labeled dendrimers were not fully conjugated with peptides, fluorescent images of the aorta were used to visualize the extravasated $(LyP\text{-}1)_4$-dendrimer-FAM. Finally, the building block synthesis approach we tested here is very flexible, can be applied with various targeting peptides, and enables a broad range of PET imaging studies for disease detection and the assessment of therapeutic delivery.

■ ASSOCIATED CONTENT

Supporting Information

SI-1: Synthesis of each building block. SI-2: MALDI spectrum of synthesized compounds. SI-3: Determination of radiochemical purity. SI-4: Biodistribution and optical study of dendrimers. SI-5: Saturation binding assay (Kd). This material is available free of charge via the Internet at http://pubs.acs.org.

■ AUTHOR INFORMATION

Corresponding Author

*Phone 530-754-9436; Fax (530) 754-5739; e-mail: kwferrara@ucdavis.edu.

Notes

The authors declare no competing financial interest.

■ ACKNOWLEDGMENTS

We acknowledge the support of the National Heart Lung and Blood Institute of the NIH as a Program of Excellence in Nanotechnology award (HHSN268201000043C), NIHR01-CA103828, NIHR01CA134659, and NIHR01CA112356, the UC Davis Mass Spectrometry facility and the Center for Molecular and Genomic Imaging (CMGI) for assistance with CT acquisition (Jennifer Fung) and with ^{64}Cu experiments (Lina Planutyte and Dave Kukis).

■ REFERENCES

(1) Libby, P. (2002) Inflammation in atherosclerosis. *Nature 420*, 868−874.

(2) Libby, P., Ridker, P. M., and Hansson, G. K. (2011) Progress and challenges in translating the biology of atherosclerosis. *Nature 473*, 317−325.

(3) Owen, D. R. J., Lindsay, A. C., Choudhury, R. P., and Fayad, Z. A. (2011) Imaging of Atherosclerosis. *Annu. Rev. Med. 62*, 25−40.

(4) Elkhawad, M., and Rudd, J. H. F. (2009) Radiotracer imaging of atherosclerotic plaque biology. *Cardiol. Clin. 27*, 345−354.

(5) Kaufmann, B. A., Sanders, J. M., Davis, C., Xie, A., Aldred, P., Sarembock, I. J., and Lindner, J. R. (2007) Molecular imaging of inflammation in atherosclerosis with targeted ultrasound detection of vascular cell adhesion molecule-1. *Circulation 116*, 276−284.

(6) Leong-Poi, H., Christiansen, J., Heppner, P., Lewis, C. W., Klibanov, A. L., Kaul, S., and Lindner, J. R. (2005) Assessment of endogenous and therapeutic arteriogenesis by contrast ultrasound molecular Imaging of integrin expression. *Circulation 111*, 3248−3254.

(7) Hyafil, F., Cornily, J. C., Feig, J. E., Gordon, R., Vucic, E., Amirbekian, V., Fisher, E. A., Fuster, V., Feldman, L. J., and Fayad, Z. A. (2007) Noninvasive detection of macrophages using a nanoparticulate contrast agent for computed tomography. *Nat. Med. 13*, 636−641.

(8) McAteer, M. A., Schneider, J. E., Ali, Z. A., Warrick, N., Bursill, C. A., von zur Muhlen, C., Greaves, D. R., Neubauer, S., Channon, K. M., and Choudhury, R. P. (2008) Magnetic resonance imaging of endothelial adhesion molecules in mouse atherosclerosis using dual-targeted microparticles of iron oxide. *Arterioscler., Thromb., Vasc. Biol. 28*, 77−83.

(9) Frias, J. C., Williams, K. J., Fisher, E. A., and Fayad, Z. A. (2004) Recombinant HDL-like nanoparticles: A specific contrast agent for MRI of atherosclerotic plaques. *J. Am. Chem. Soc. 126*, 16316−16317.

(10) Kietselaer, B. L., Reutelingsperger, C. P., Heidendal, G. A., Daemen, M. J., Mess, W. H., Hofstra, L., and Narula, J. (2004) Noninvasive detection of plaque instability with use of radiolabeled annexin A5 in patients with carotid-artery atherosclerosis. *New Engl. J. Med. 350*, 1472−1473.

(11) Broisat, A., Hernot, S., Toczek, J., De Vos, J., Riou, L. M., Martin, S., Ahmadi, M., Thielens, N., Wernery, U., Caveliers, V., Muyldermans, S., Lahoutte, T., Fagret, D., Ghezzi, C., and Devoogdt, N. (2012) Nanobodies targeting mouse/human VCAM1 for the nuclear imaging of atherosclerotic lesions. *Circ. Res. 110*, 927−937.

(12) Wykrzykowska, J., Lehman, S., Williams, G., Parker, J. A., Palmer, M. R., Varkey, S., Kolodny, G., and Laham, R. (2009) Imaging of inflamed and vulnerable plaque in coronary arteries with ^{18}F-FDG PET/CT in patients with suppression of myocardial uptake using a low-carbohydrate, high-fat preparation. *J. Nucl. Med. 50*, 563−568.

(13) Rudd, J. H. F., Myers, K. S., Bansilal, S., Machac, J., Pinto, C. A., Tong, C., Rafique, A., Hargeaves, R., Farkouh, M., Fuster, V., and Fayad, Z. A. (2008) Atherosclerosis inflammation Imaging with ^{18}F-

FDG PET: Carotid, iliac, and femoral uptake reproducibility, quantification methods, and recommendations. *J. Nucl. Med. 49*, 871−878.
(14) Razzouk, L., and Farkouh, M. E. (2009) Imaging outcomes in cardiovascular clinical trials. *Nat. Rev. Cardiol. 6*, 524−531.
(15) Shaw, S. Y. (2009) Molecular imaging in cardiovascular disease: targets and opportunities. *Nat. Rev. Cardiol. 6*, 569−579.
(16) Dobrucki, L. W., and Sinusas, A. J. (2010) PET and SPECT in cardiovascular molecular imaging. *Nat. Rev. Cardiol. 7*, 38−47.
(17) Nahrendorf, M., Zhang, H. W., Hembrador, S., Panizzi, P., Sosnovik, D. E., Aikawa, E., Libby, P., Swirski, F. K., and Weissleder, R. (2008) Nanoparticle PET-CT imaging of macrophages in inflammatory atherosclerosis. *Circulation 117*, 379−387.
(18) Saraste, A., Nekolla, S. G., and Schwaiger, M. (2009) Cardiovascular molecular imaging: an overview. *Cardiovasc. Res. 83*, 643−652.
(19) Rudd, J. H., Warburton, E. A., Fryer, T. D., Gillard, J. H., Graves, M. J., Clark, J. C., Pickard, J. D., Kirkpatrick, P. J., and Weissberg, P. L. (2002) Carotid atherosclerotic plaque inflammation imaged using (18)Fluorodeoxyglucose positron emission tomography ((18)FDG-PET) and high resolution magnetic resonance (HRMR). *Stroke 33*, 362−362.
(20) Tawakol, A., Migrino, R. Q., Bashian, G. G., Bedri, S., Vermylen, D., Cury, R. C., Yates, D., LaMuraglia, G. M., Furie, K., Houser, S., Gewirtz, H., Muller, J. E., Brady, T. J., and Fischman, A. J. (2006) In vivo ^{18}F-fluorodeoxyglucose positron emission tomography imaging provides a noninvasive measure of carotid plaque inflammation in patients. *J. Am. Coll. Cardiol. 48*, 1818−1824.
(21) Nahrendorf, M., Keliher, E., Panizzi, P., Zhang, H. W., Hembrador, S., Figueiredo, J. L., Aikawa, E., Kelly, K., Libby, P., and Weissleder, R. (2009) ^{18}F−4V for PET-CT imaging of VCAM-1 expression in atherosclerosis. *J. Am. Coll. Cardiol. Img. 2*, 1213−1222.
(22) Fogal, V., Zhang, L., Krajewski, S., and Ruoslahti, E. (2008) Mitochondrial/cell-surface protein p32/gC1qR as a molecular target in tumor cells and tumor stroma. *Cancer Res. 68*, 7210−7218.
(23) Laakkonen, P., Porkka, K., Hoffman, J. A., and Ruoslahti, E. (2002) A tumor-homing peptide with a targeting specificity related to lymphatic vessels. *Nat. Med. 8*, 751−755.
(24) Uchida, M., Kosuge, H., Terashima, M., Willits, D. A., Liepold, L. O., Young, M. J., McConnell, M. V., and Douglas, T. (2011) Protein cage nanoparticles bearing the LyP-1 peptide for enhanced imaging of macrophage-rich vascular lesions. *ACS Nano 5*, 2493−2502.
(25) Hamzah, J., Kotamraju, V. R., Seo, J. W., Agemy, L., Fogal, V., Mahakian, L. M., Peters, D., Roth, L., Gagnon, M. K. J., Ferrara, K. W., and Ruoslahti, E. (2011) Specific penetration and accumulation of a homing peptide within atherosclerotic plaques of apolipoprotein E-deficient mice. *Proc. Natl. Acad. Sci. U. S. A. 108*, 7154−7159.
(26) Lempens, E. H. M., Merkx, M., Tirrell, M., and Meijer, E. W. (2011) Dendrimer display of tumor-homing peptides. *Bioconjugate Chem. 22*, 397−405.
(27) Dijkgraaf, I., Rijnders, A. Y., Soede, A., Dechesne, A. C., van Esse, G. W., Brouwer, A. J., Corstens, F. H. M., Boerman, O. C., Rijkers, D. T. S., and Liskamp, R. M. J. (2007) Synthesis of DOTA-conjugated multivalent cyclic-RGD peptide dendrimers via 1,3-dipolar cycloaddition and their biological evaluation: implications for tumor targeting and tumor imaging purposes. *Org. Biomol. Chem. 5*, 935−944.
(28) Franc, G., and Kakkar, A. (2008) Dendrimer design using Cu(I)-catalyzed alkyne-azide "click-chemistry". *Chem. Commun.*, 5267−5276.
(29) Gray, B. P., Li, S. Z., and Brown, K. C. (2013) From phage display to nanoparticle delivery: functionalizing liposomes with multivalent peptides improves targeting to a cancer biomarker. *Bioconjugate Chem. 24*, 85−96.
(30) Brabez, N., Saunders, K., Nguyen, K. L., Jayasundera, T., Weber, C., Lynch, R. M., Chassaing, G., Lavielle, S., and Hruby, V. J. (2013) Multivalent interactions: synthesis and evaluation of melanotropin multimers-tools for melanoma targeting. *ACS Med. Chem. Lett. 4*, 98−102.
(31) Helms, B. A., Reulen, S. W. A., Nijhuis, S., de Graaf-Heuvelmans, P. T. H. M., Merkx, M., and Meijer, E. W. (2009) High-affinity peptide-based collagen targeting using synthetic phage mimics: from phage display to dendrimer display. *J. Am. Chem. Soc. 131*, 11683−11685.
(32) Okuda, T., Kawakami, S., Akimoto, N., Niidome, T., Yamashita, F., and Hashida, M. (2006) PEGylated lysine dendrimers for tumor-selective targeting after intravenous injection in tumor-bearing mice. *J. Controlled Release 116*, 330−336.
(33) Kaminskas, L. M., Kelly, B. D., McLeod, V. M., Boyd, B. J., Krippner, G. Y., Williams, E. D., and Porter, C. J. H. (2009) Pharmacokinetics and tumor disposition of PEGylated, methotrexate conjugated poly-L-lysine dendrimers. *Mol. Pharmaceutics 6*, 1190−1204.
(34) Ohsaki, M., Okuda, T., Wada, A., Hirayama, T., Niidome, T., and Aoyagi, H. (2002) In vitro gene transfection using dendritic poly(L-lysine). *Bioconjugate Chem. 13*, 510−517.
(35) Gaertner, H. F., Cerini, F., Kamath, A., Rochat, A. F., Siegrist, C. A., Menin, L., and Hartley, O. (2011) Efficient orthogonal bioconjugation of dendrimers for synthesis of bioactive nanoparticles. *Bioconjugate Chem. 22*, 1103−1114.
(36) Anderson, C. J., and Ferdani, R. (2009) Copper-64 radiopharmaceuticals for PET imaging of cancer: advances in preclinical and clinical research. *Cancer Biother. Radiopharm. 24*, 379−393.
(37) Qin, S. P., Seo, J. W., Zhang, H., Qi, J., Curry, F. R. E., and Ferrara, K. W. (2010) An imaging-driven model for liposomal stability and circulation. *Mol. Pharmaceutics 7*, 12−21.
(38) Seo, J. W., Zhang, H., Kukis, D. L., Meares, C. F., and Ferrara, K. W. (2008) A novel method to label preformed liposomes with ^{64}Cu positron emission tomography (PET) imaging. *Bioconjugate Chem. 19*, 2577−2584.
(39) Kukis, D. L., Li, M., and Meares, C. F. (1993) Selectivity of antibody-chelate conjugates for binding copper in the presence of competing metals. *Inorg. Chem. 32*, 3981−3982.
(40) Obata, A., Kasamatsu, S., McCarthy, D. W., Welch, M. J., Saji, H., Yonekura, Y., and Fujibayashi, Y. (2003) Production of therapeutic quantities of Cu-64 using a 12 MeV cyclotron. *Nucl. Med. Biol. 30*, 535−539.
(41) McCarthy, D. W., Shefer, R. E., Klinkowstein, R. E., Bass, L. A., Margeneau, W. H., Cutler, C. S., Anderson, C. J., and Welch, M. J. (1997) Efficient production of high specific activity Cu-64 using a biomedical cyclotron. *Nucl. Med. Biol. 24*, 35−43.
(42) Chen, L. A., Mccrate, J. M., Lee, J. C. M., and Li, H. (2011) The role of surface charge on the uptake and biocompatibility of hydroxyapatite nanoparticles with osteoblast cells. *Nanotechnology 22*.
(43) Chung, T. H., Wu, S. H., Yao, M., Lu, C. W., Lin, Y. S., Hung, Y., Mou, C. Y., Chen, Y. C., and Huang, D. M. (2007) The effect of surface charge on the uptake and biological function of mesoporous silica nanoparticles 3T3-L1 cells and human mesenchymal stem cells. *Biomaterials 28*, 2959−2966.
(44) Jiang, X. E., Dausend, J., Hafner, M., Musyanovych, A., Rocker, C., Landfester, K., Mailander, V., and Nienhaus, G. U. (2010) Specific effects of surface amines on polystyrene nanoparticles in their interactions with mesenchymal stem cells. *Biomacromolecules 11*, 748−753.